Polarization-Based Fiber Optic System for Debris Flow Early Warning: On-Field Demonstration

Polarization-Based Fiber Optic System for Debris Flow Early Warning: On-Field Demonstration

Saverio Pellegrini, Giuseppe Rizzelli, Marco Barla, and Roberto Gaudino, *Senior Member, IEEE*

***Abstract*—Naturally occurring mass transport events can endanger human life and infrastructure integrity, especially in mountain areas often affected by landslides, debris flows, and avalanches. Currently available hazard detection systems can greatly help with the timely warning (within a few seconds) of ongoing, potentially dangerous events, but can often be inaccurate, unreliable and, due to the need for in-situ power supply, difficult to operate. Modern optical fiber sensing techniques, on the other hand, can provide exceptional accuracy but require longer measurement time and increased complexity and cost, which makes them unsuitable for such time- and cost-sensitive applications. In this paper, we present an on-field demonstration of a previously developed polarization-based optical fiber early-warning system. A mountain gully in the Valle d'Aosta region, in Italy, is used as a validation testbed to show the reliability of our approach in detecting anomalous vibration phenomena, and its robustness against the background noise associated, for instance, with car traffic or animal wildlife in the monitored area. Our findings show that the rate of variation of the state of polarization induced by real-life, hazardous rockfall events on the optical fiber is orders of magnitudes higher than the average variation rate recorded in normal conditions, thus making the proposed system a promising alternative in the mountain hazards sensors world. Moreover, we show that the system has great potential for increased accuracy in the monitoring of event dynamics by using different optical fibers in separate sections of the site, which can also be a source of additional cost reduction.**

***Index Terms*—Optical fibers, polarization, birefringence, rockfalls, monitoring and alarm system.**

I. Introduction

MOUNTAIN slopes are increasingly affected by destructive events such as rockfalls, landslides, avalanches, and debris flows. When these phenomena occur near inhabited areas, monitoring systems with response times of a few seconds, for fast detection and warning/alarm generation, can mitigate their consequences and reduce the risks for the local communities, minimizing damages to public or private properties and disruptions to local services such as transportation and utilities. For instance, assuming a debris flow with a typical speed of 36 km/h (i.e. 10 m/s) and a fiber placed across the gully 500 m above the interrogator, the system response time of 10 seconds would enable the alarm to be generated 40 seconds before the event arrives at the interrogator location. This would give enough time to block road traffic using, for example, a traffic light.

In this scenario, geotechnical engineering solutions have been developed in recent times, usually employing sensors based on different technologies [1], [2] such as geophones or seismometers [3]. More recently, systems based on radars, lidars, or infrared cameras [4], [5], [6], [7] have also been proposed and installed. Generally speaking, currently available solutions are usually limited by one or more of the following reasons: i) small coverage area (usually in specific exact locations); ii) low visibility that can hinder detection capability; iii) need for power supplied directly on-site; iv) visual impact in areas often subject to environmental restrictions, such as national parks or natural reserves.

In the quest for a technology that can help overcome the shortcomings of commercial solutions, optical fibers have recently attracted a great deal of interest [8], [9], thanks to their very high sensitivity to vibrational phenomena and potential for very large coverage. Fiber-based optical techniques range from discrete sensing, usually employing Fiber-Bragg gratings (FBGs) to sense only in specific locations where the FBGs are placed, to distributed sensing [10], [11], [12], exploiting Brillouin, Raman or Rayleigh [13], [14], [15] backscattering effects to turn the whole fiber into a sensor, and interferometric techniques such as those presented in [16], [17], [18]. Unlike traditional geotechnical systems, optical fiber sensing techniques can provide i) extremely high accuracy with the possibility to locate the event; ii) high reliability with exceptional sensitivity to temperature, strain and vibrations; iii) large coverage areas with sensing capabilities over tens of km; iv) no need for local power supply as only the fiber needs to be installed on-site, whereas the interrogator can be placed in a convenient, controlled location; v) no visual impact as the fiber can be buried underground. However, the main drawbacks of advanced distributed fiber-based monitoring systems are usually the high cost ($>$ 100 k€), and the relatively long measurement time (tens of seconds required for averaging over several backscattering traces) that prevent their use as early warning systems.

In our latest works [19], [20], [21] we presented a "quasi-distributed" approach where the change rate of the state of polarization (SOP) of light is monitored at the output of an optical fiber to measure the level of vibrational perturbation along the fiber. The acquired information is the result of a spatial integration of

Manuscript received 5 April 2024; revised 11 May 2024; accepted 15 May 2024. Date of publication 20 May 2024; date of current version 28 May 2024. *(Corresponding author: Saverio Pellegrini.)*

Saverio Pellegrini, Giuseppe Rizzelli, and Roberto Gaudino are with the Dipartimento di Elettronica e Telecomunicazioni (DET), Politecnico di Torino, 10129 Torino, Italy (e-mail: saverio.pellegrini@polito; giuseppe.rizzelli@polito.it; roberto.gaudino@polito.it).

Marco Barla is with the Department of Structural, Geotechnical and Building Engineering (DISEG), Politecnico di Torino, 10129 Torino, Italy (e-mail: marco.barla@polito.it).

Digital Object Identifier 10.1109/JPHOT.2024.3403159

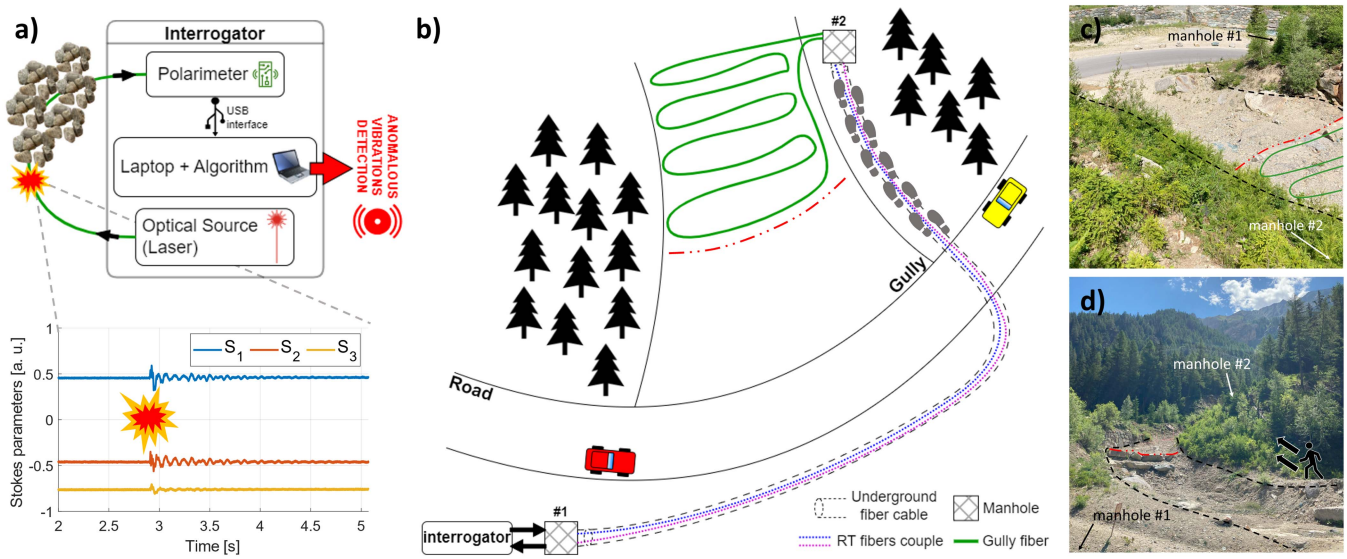

Fig. 1. (a) Block diagram of the interrogator, and working principle of the polarization-based detection system. (b) Schematic representation of the monitored site with fibers layout. (c) View of the gully from manhole #2 and (d) from manhole #1. The dashed blue and violet lines are the fibers selected for the round-trip, contained inside the black dashed cylinder representing the underground cable. The green line shows the fiber configuration on the surface. Footsteps indicate a semi-exposed portion of the cable in a passageway in the woods. The red line shows the bottom limit of the fiber installation. The black dotted lines in (c) and (d) show the lateral edges of the gully.

all the SOP variations along the entire length of the fiber and, while not suitable for localization, the fiber can be extremely long (up to hundreds of kilometers) and can thus be used to monitor vast geographical areas. The idea is based on the well-known concept of stress-induced fiber birefringence [22], [23], [24] that makes the SOP very sensitive to the mechanical stresses and vibrations [25], [26], [27], [28] occurring on the fiber. A large number of papers have demonstrated the reliability of polarization-based monitoring systems, particularly in undersea [29] and metropolitan [30], [31] situations. Polarization-based sensing allows a notable cost reduction compared to traditional optical sensing methods as it does not require sophisticated opto-electronics instrumentation, combined with the aforementioned benefits compared to geotechnical monitoring systems. Fig. 1(a) summarizes the working principle of the proposed sensing scheme, of which a detailed description is provided in [19]. The effect of rockfalls-generated mechanical vibrations over the optical fiber (depicted as the green line in Fig. 1(a)) is shown on the Stokes parameters evolution in the same Figure. The interrogator contains all the necessary hardware to gather, process the data, and alarm the surrounding area when needed. Further details on detection algorithms will be provided in this paper, while a techno-economic comparison of the state of the art in mountain early warning solutions with standard and polarization-based optical fiber techniques can be found in [19].

In this paper we extend the analysis of the monitoring system proposed in [19] with on-field experiments, performed over a mountain gully, in order to test in a real environment the detection algorithm which we previously studied only on a reduced scale laboratory model. We installed several fibers along the mountain gully and connected them to an SOP interrogator. Then, we emulated the downhill fall of some heavy material and show that by properly setting the algorithm's main parameters, the normal/threatening conditions can be properly identified, thus demonstrating for the first time a promising realistic application of our sensing method. We focus on the validation of our approach in normal conditions when vehicles, passers-by and animal wildlife could produce false alarms and thus reduce the reliability of the threat detection system.

The manuscript is organized as follows: in Section II, a description of the monitoring site in the Italian Valle d'Aosta region and of the fiber arrangement is provided. Section III includes the results of the characterization of the normal conditions (when no event is generated) induced by everyday life events (e.g. traffic, weather, animals). In Section IV we show the performance of the detection algorithm when rockfall-like hazards are emulated on a single fiber, and in a configuration with two separate fibers used to monitor two different portions of the site. Lastly, in Section V we provide a final discussion and conclusions.

II. On-Field Setup

The test site selected for this work is a mountain gully in Cogne, Valle d'Aosta, Italy. One cable containing a bundle of 24 standard single mode fibers (SMF) has been installed along a roadway approximately half a meter underground, in the same housing used for the common power line. Fig. 1(b)–(d) show the experimental scenario, providing pictures of the site, while Fig. 1(a) shows the interrogator hardware. The green fiber displaced over the gully (also standard G.652 SMF) in Fig. 1(b) is subject to dangerous events and, through the underground fiber cable, connects to the interrogator, which processes the SOP delivering, if necessary, alarms. As shown in Fig. 1(b) and (c), the roadway is in a particularly dangerous location at the bottom of the gully, at about 30 m from the depicted red line. This is a fundamental aspect of this work, since a flowing mass event

would hit the road and would be potentially extremely dangerous for cars and people in the area. An early warning system should then be connected to a signaling system to restrict access to the dangerous area after detecting the threat. On the other hand, at specific times of the year, this area is very populated: bikers, hikers, or cars could generate spurious events in proximity of the fibers, possibly causing false alarms. In fact, as shown in Fig. 1(b) and (d), the underground fiber cable path crosses the road and connects to manhole #2 through a walkway (footsteps), where it runs inside a corrugated hose that is only partially buried and is thus semi-exposed. The gully fiber, in green in Fig. 1(b) and (c), is the actual sensing-dedicated portion of the whole fiber path, as it is laid out over the area where real hazards can occur. In this work, we did not bury it underground as we envisioned in [19], to analyze the worst noise conditions, as the sensor is completely exposed to any surrounding environment agent. We define noise as the small SOP variations that occur when the fiber is completely at rest, i.e. in normal conditions, and environment-induced noise as the SOP variations due to environmental effects such as road traffic, weather conditions (e.g. wind, rain), people, and animals walking in the vicinity of the fiber, and all other effects that can occur during a normal day but are not related to dangerous events and should not trigger an alarm. Access to the cable is provided at both ends by two manholes (#1 and #2). The gully fiber is connected to two of the 24 fibers inside the cable at the manhole #2. The fiber pair connects the interrogator in Fig. 1(a) with the fiber in the gully in a round-trip configuration, and will thus be referred to as round-trip (RT) fiber pair. The selected RT fibers are highlighted in Fig. 1(b) as blue and violet dashed lines.

The gully fiber is arranged in an S-shaped configuration (i.e. laid in a serpentine pattern) as already tested in [19]. Experiments considering gully fiber lengths of 40 m and 80 m have been carried out and will be presented in the following Sections. The underground cable is about 200 m long, for a total RT fibers length of 400 m. The whole fiber length is then approximately 440 m and 480 m when the gully fiber is connected, respectively. This configuration has been chosen to emulate a situation where the interrogator is placed in a secure location, such as a street cabinet, that can be far from the monitoring site.

Fig. 1(a) shows the hardware used for the experiments. The interrogator is connected to the RT fibers at manhole #1 location. The optical source is a low-cost (a few hundred €) Fabry-Perot laser emitting continuous wave (CW) light at 1550 nm into one of the RT fibers. In a loopback kind of configuration, the optical signal travels to manhole #2, through the gully fiber (when connected) and then back to the interrogator through the second RT fiber, where it is collected by a polarimeter (Novoptel PM1000) with a photodetector covering an extended C-band in the 1501–1565 nm range, analog bandwidth of 25 MHz and acceptable input optical power in the range from −36 dBm to +4 dBm. The polarimeter transfers to the laptop via USB cable the SOP as a vector $\vec{S}[k]$ of three Stokes parameters S_1, S_2, S_3 at discrete time instants $\vec{S}[k] = (S_1[k], S_2[k], S_3[k])$, where k is the discrete time index. A low sampling frequency $f_s = 95.4$ Hz proved to be sufficient for our purposes, due to the low frequency content associated with real-life mechanical events [32]. For this reason, simpler and cheaper (<6 k€) devices available on the market can be used in a real installation, instead of the high-end lab-grade polarimeter employed for this work.

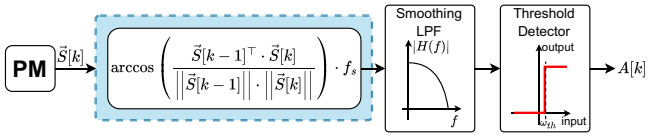

Fig. 2. Scheme of the DSP chain employed to compute and monitor the SOPAS.

III. Environment-Induced Noise Analysis

The effects that natural environment has on the fiber and therefore on the detection capabilities of the proposed system need to be well characterized to fully understand its level of reliability in an on-field scenario on a real mountain slope. Results shown in this and the following Sections are obtained by analyzing the State Of Polarization Angular Speed (SOPAS). This metric is computed starting from the Stokes vector $\vec{S}[k]$ discrete time series provided by the polarimeter (PM), and accounts for the angular change rate between consecutive SOP samples on the Poincaré sphere. In our previous work [19] we demonstrated that this metric can be used reliably to detect different kinds of hazardous events reproduced in our laboratory environment. Fig. 2 shows the functional diagram of the DSP algorithm used to compute and monitor the SOPAS and, through a threshold-based detector, deliver an alarm signal $A[k]$ when above threshold SOPAS values are observed, likely related to dangerous mechanical events. The dashed light-blue rectangle in Fig. 2 shows how the SOPAS is evaluated. A Low Pass Filter (LPF), i.e. a moving average (or smoothing) filter, is applied to the data stream, enhancing the detection capability of the threshold-based detector. The filtered SOPAS is then compared with a previously fixed threshold ω_{th}, to decide for alarm (above threshold) or quiet (below threshold) conditions. In this paper, the length of the moving average window is set to one second unless otherwise specified. The analysis that follows refers to the metric computed at the output of the LPF.

To characterize in detail the effect of environmental noise on the system, different configurations are considered. First, we focus on the characterization of the noise level considering only the RT fiber couple inside the cable. In this first analysis, the gully fiber is not connected and the loop is closed at the manhole #2 location through a patchcord connecting the two RT fibers. In this configuration we also tested our algorithm in a somewhat critical situation where anomalous vibrations can be generated by animals, hikers or bikers stepping over the semi-exposed fiber segment installed on the side of the gully up to manhole #2, in an area where the hazard would not be sensed and no other events should generate a false alarm. The results are shown in Fig. 3 as a comparison between the condition where we introduced SOP perturbations by walking on the fiber (W) and the quiet state (Q) without walking. The two histograms show the distribution of the SOPAS intensity samples acquired over two minutes (which is the time spent walking over the fiber) and

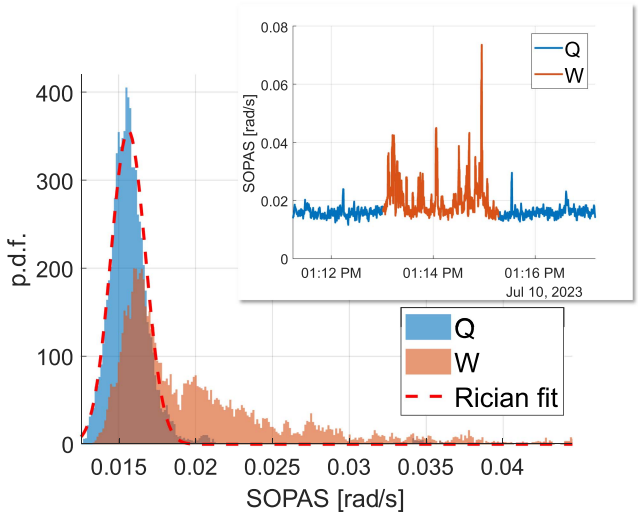

Fig. 3. Distribution of SOPAS samples for the walking (W) and quiet (Q) case, normalized to show probability density functions. Red-dashed line shows the theoretical Rician pdf fit on the Q distribution. The inset shows the corresponding SOPAS evolution in time.

are normalized to obtain a probability density function (pdf). For the Q distribution, a fit with the theoretical Rician probability density function is provided, showing good correspondence. Since the SOPAS intensity is higher when the effect of walking on the fiber is present, the corresponding distribution is slightly more spread on the x-axis. Nevertheless, the two pdf overlap for the most part, showing that the generated perturbations are relatively small. We believe this is the first important result of our analysis as it clearly demonstrates that false alarms due to common and non-threatening events are unlikely to be generated by our system, after a proper setting of the ω_{th} value. Moreover, as it will become clear in the next Section, the intensity shown in Fig. 3 is much smaller than that of mass transport phenomena and can be easily disregarded by setting a proper alarm threshold on the SOPAS.

The configuration with only the RT fiber is discussed as a baseline since it is not significant in the aim to detect anomalous conditions occurring inside the gully. We now introduce the more relevant cases where a section of SMF is added to the underground portion and deployed on the surface of the gully. This is the segment actually dedicated to the sensing of potentially dangerous rockfall events. We deployed a 40 m and then an 80 m long piece of fiber in the gully. Fig. 4(a) shows the distributions of the SOPAS samples acquired in the configurations with the added gully fibers, and compares them to the distributions shown in Fig. 3 for the RT fiber only. Please note that all the distributions refer to SOPAS acquisitions over 20 minutes except that for the walking case (orange histogram) that lasted 2 minutes only. The RT fibers are buried, thus well isolated from external agents that may affect the SOP. This explains why the blue (RT, Q) distribution is well separated from the purple (RT + Gully fiber 40 m) and green (RT + Gully fiber 80 m) ones which instead refer to the addition of gully fibers, completely exposed to the mountain environment. The mean value of the SOPAS increases with the fiber length, showing that the amount of noise rises slightly when a longer fiber is deployed, as a longer portion is exposed to external events. In our on-field test this effect is partly due to the fact that the sensing fiber is laid onto the gully surface without being secured and, therefore, additional effects due to the weather (e.g. wind) or ground topology can contribute to the overall noise floor. Nevertheless, we have examined the behavior of the system with the longer fiber in the gully over several hours, thus characterizing the inherent noise level of the configuration with 80 m SMF. Fig. 4(b) shows the 12-hour overnight evolution of the SOPAS, highlighting a consistent average value of around 0.07 rad/s. It shows also some spurious peaks with a duration of 1–2 seconds and intensity comparable, for the majority of them, to the walking case shown in the inset of Fig. 3, confirming that our system, through an appropriate selection of the threshold ω_{th}, can be made robust to non-dangerous events with SOP variation amplitudes well below those that would be produced during a mass transport phenomenon (see Section IV). Another possible source of false alarms in our deployed monitoring system could be related to vehicles driving across the RT fibers installed underground perpendicular to the traffic direction. Works such as [33], [34] have shown the effect of low frequency vibrations, mainly in the range from 3 to 20 Hz, induced on underground metropolitan fibers by moving vehicles, to which DAS systems are particularly sensitive. We characterized the effect of traffic on the SOPAS in the configuration with 40 m gully fiber added to the RT fibers. Fig. 5 shows the acquired SOPAS traces processed with a moving average window of 0.1 s duration, for different numbers of vehicles driving by on the road. In all five cases there is no significant evidence of SOP variation due to traffic, confirming that the installation is robust and the system would not respond with wrong detection alarms to everyday conditions.

IV. Anomalous Events Detection Analysis

In this Section, we move from the characterization of the normal operating conditions of our installed monitoring system to the on-field measurements of anomalous events. As we are not able to generate realistic mass transport events, we emulated the vibrational effects associated with solid material hitting the fiber by releasing several types of balls from the top and letting them roll on the 40 m gully fiber. Specifically, we launched 6 small spheres (750 grams, about 7 cm in diameter) and a larger one (a 3 kg medical ball, 19 cm in diameter). Please note that this methodology was not intended to mimic real catastrophic rockfall episodes, but rather to emulate out-of-the-ordinary situations, and was selected to calibrate the system and demonstrate that, given the great difference between normal conditions and exceptional circumstances, through proper setting of the algorithm parameters, false alarms can be reasonably prevented. The situations that will be discussed are pessimistic in terms of intensity if compared to a real flowing mass event occurring over the gully, which would be much more intense and also longer in time. In the following two subsections we will discuss the system detection capabilities when monitoring one fiber only, or two fibers simultaneously.

A. Single Fiber Configuration

The aforementioned events were generated on the configuration with the 40 m gully fiber. The SOPAS traces of eight events

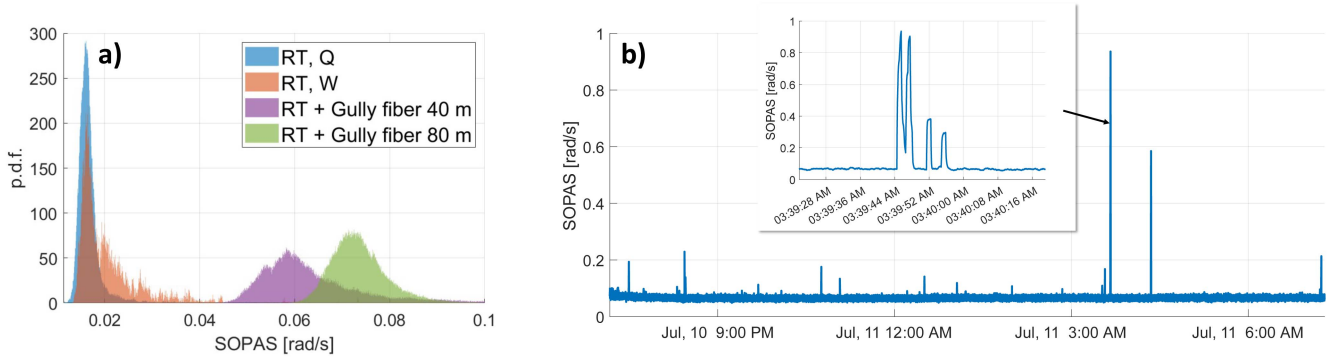

Fig. 4. (a) Distribution of SOPAS samples in the walking (orange) and quiet (blue) case with RT fibers only, in the quiet state with 40 m gully fiber (purple), and in the quiet state with 80 m gully fiber (green). (b) SOPAS time evolution over 12 hours in the configuration with 80 m gully fiber.

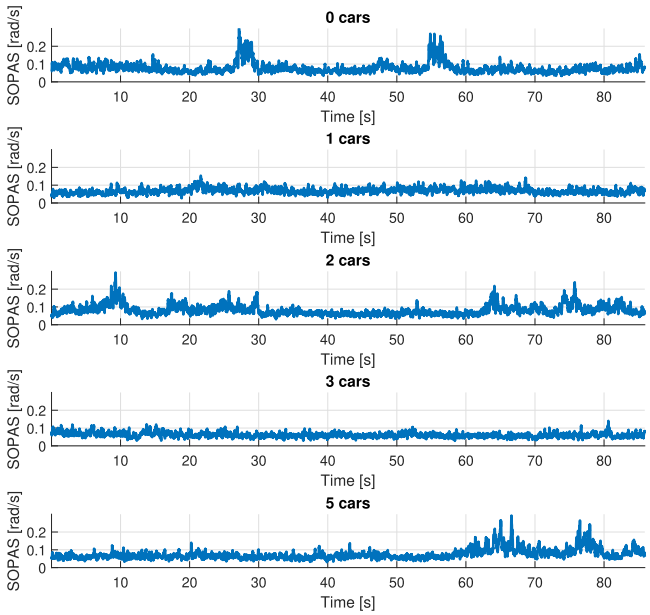

Fig. 5. SOPAS traces acquired during the crossing of RT fibers of 0, 1, 2, 3, and 5 vehicles. The fiber configuration considers the 40 m gully fiber.

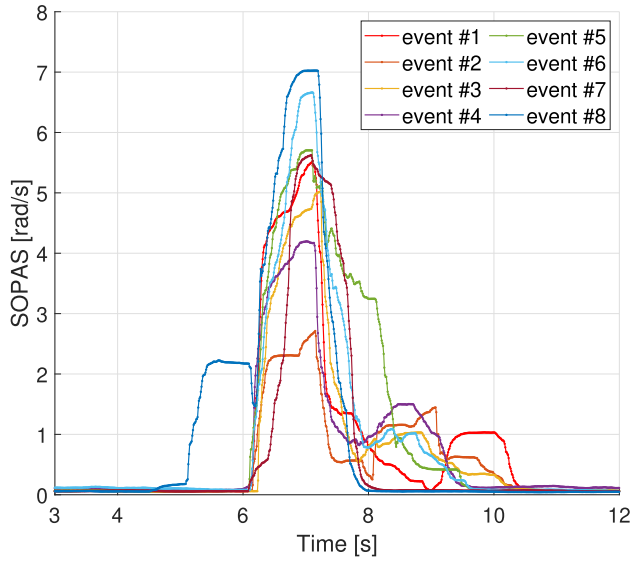

Fig. 6. Eight different SOPAS traces associated with out-of-the-ordinary events generated over the 40 m long gully fiber.

are reported in Fig. 6. On average, the SOPAS peak values are between 3 rad/s and 7 rad/s, two orders of magnitude higher than the mean values shown in Fig. 4(a) for the 40 m (0.047 rad/s) and 80 m (0.071 rad/s) gully fiber added to the RT pair. Realistically, we can assume that actual debris flows generate even higher SOPAS, thus these results suggest that the proposed system can be operated to produce only correct detection (CD) without any false alarm (FA) or missed detection (MD). MD occurs when the threshold is set too high and the events do not trigger the alarm while the opposite case, FA, occurs when the threshold is too low and the noise triggers the alarm instead of true events. 100% CDs, on the other hand, is the desired output of an alarm system, without any occurrence of MDs nor FAs.

In a scenario where actual flowing masses strike the fibers displaced on the gully surface, it's reasonable to assume that not only their intensity is higher than that shown in Fig. 6, but also their duration is much longer than the 2–3 seconds of the events that we were able to generate. Thus, by also monitoring the events duration, whenever an above-threshold condition is detected, it would be possible to further distinguish between real flowing masses and non-dangerous events generated spuriously. An example is represented by the two highest SOPAS spikes in Fig. 4(b). The peak angular speed in these two cases, although much lower than what we expect in realistic hazardous phenomena, is comparable to some of the peak values in Fig. 6. Nevertheless, these spurious noise spikes have a limited duration, about 2 seconds each, a completely different time scale if compared to true debris flow events, whose duration is in the order of tens of seconds [35]. In this context, considering the 12 hours acquisition in Fig. 4(b), the red curve in Fig. 7 shows the total duration of FA alarms, i.e. the total time that SOPAS samples have been above the threshold, versus selected threshold. The upper x-axis limit is set to 0.93 rad/s, which is the highest value of SOPAS during the night acquisition. The red curve depicts an interesting scenario for the detection system, since even for thresholds one order of magnitude smaller (0.4

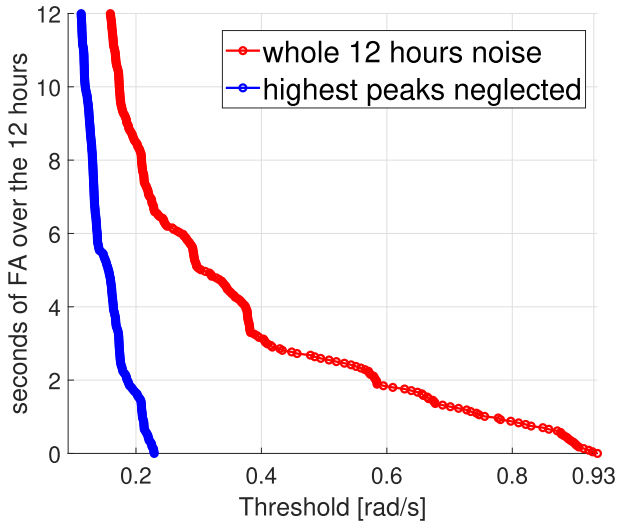

Fig. 7. Seconds of FA over the 12 hours SOPAS acquisition as a function of the threshold value. The red curve has been obtained considering the whole 80 m fiber overnight acquisition, the blue one has been obtained neglecting the two highest spurious spikes.

to 0.6 rad/s) than the SOPAS peak values associated with the events in Fig. 6, the system would deliver about 2 to 3 seconds of FA in 12 hours, meaning that spurious noise peaks can be easily disregarded by fixing a time-duration threshold around 2 seconds.

Moreover, the two noise spikes measured overnight, might not be related to actual events, but to the specific limitations of our experimental setup (e.g. gully fiber not properly deployed), which would be minimized in a real installation. By neglecting the two peaks, the blue curve in Fig. 7 is obtained. In this case, all the threshold values above 0.23 rad/s will not produce any FA, allowing for a more robust detection. Generally speaking, employing a time-duration threshold increases the detection time by a delay equal to the threshold value. If an alarm generated for monitoring gullies is delayed by about 2 seconds, it would not be critically harmful. Gullies can be several hundred meters long and the gully fibers can be moved further uphill to compensate for it, if needed.

A potential approach for establishing operating thresholds would first involve acquiring the SOP data over an extended timeframe (weeks, months) to ensure greater statistical relevance, and subsequently repeat the analysis discussed above. The red curve depicted in Fig. 7 would be generated again, allowing for the determination of an acceptable total duration of false alarms over the entire acquisition period. The duration-time and SOPAS thresholds could then be applied accordingly. Furthermore, to account for the possibility of fiber damage, occurring as a result of massive events, a straightforward enhancement to the algorithm, such as monitoring the $S_0[k]$ parameter associated with the received power, can enable the detection of fiber cuts.

B. Two Fibers Detection System

In our proposed system, information on SOP variation can be obtained only at the fiber output and the vibrations in each point of the fiber are integrated over its entire length, thus event localization cannot be implemented. However, in [19], [21] we discuss a multi-fiber configuration of our system as a possible solution for simultaneously improving the spatial resolution and reducing the probability of false alarms. Monitoring several different fibers deployed in different sections of the site enables a rough estimation of the position of the detected event, and moreover, it allows alarm triggering only when it has been detected in more than one section. Furthermore, the system can be made more cost-effective by using an optical switch to sequentially interrogate the different fibers, which would allow for the use of a single polarimeter. However, in this first validation of the multi-fiber configuration, we added an optical splitter at the laser output and deployed two optical SMFs, each 40 meters long, connected to two dedicated polarimeters with a synchronized time base. The fibers layout on the gully is depicted in Fig. 8. Similar SOPAS measurements as in Section IV have been carried out during the fall of the same 6 small and 1 bigger spherical masses. Four SOPAS traces are shown in Fig. 9 for four different

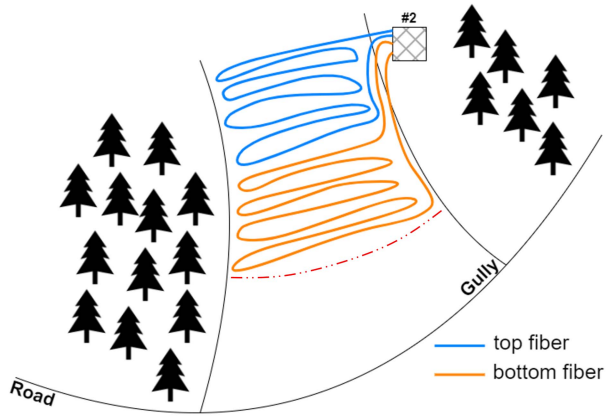

Fig. 8. Two-fiber detection system setup showing the top (blue) and the bottom (orange) fiber.

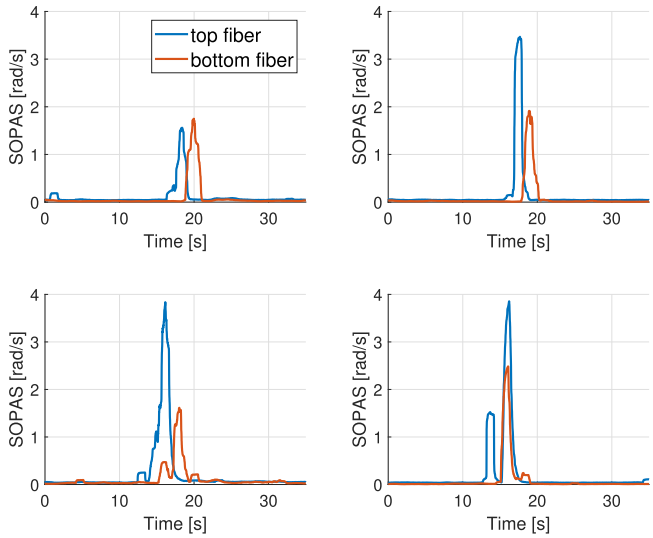

Fig. 9. SOPAS measured during four different launches in the two-fiber configuration.

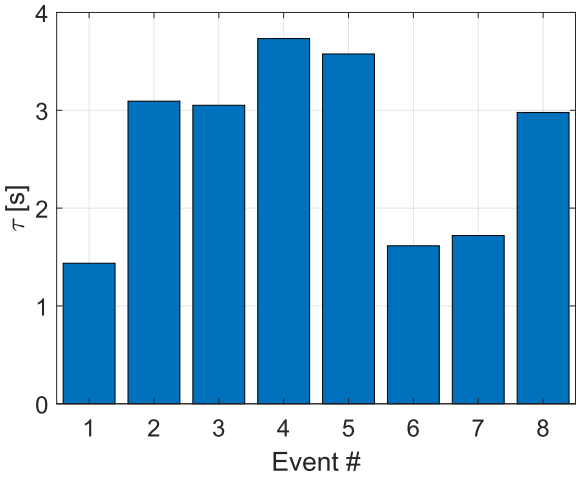

Fig. 10. Bar plot showing on the y-axis the delays computed by means of cross-correlation in between the SOPAS traces acquired on the two fibers. The related events are identified just as numbers on the x-axis.

events. As the two sections of the gully monitored by the two fibers are displaced by a few meters, the SOPAS time evolution shows two different peaks a few seconds apart. The first peak shows a clear detection of the event on the top (blue) fiber, whereas the second peak shows that the emulated mass transport event has moved downhill onto the second fiber. By applying the same threshold-based detection algorithm discussed in IV-A, for the single fiber scheme, the overall system performance in terms of false alarm reduction, can be greatly improved in this scenario, by generating an alarm only when the SOPAS falls above the threshold on both fibers. Moreover, the angular speed peaks are always delayed by an amount of time that depends on the known distance between the two fibers (about one to two seconds in our experiment), thus an estimate of the speed of the sensed event can be obtained by computing the cross-correlation between the two measured SOPAS traces. The results concerning the time-delay estimate τ of the same event occurring on the two fibers are shown in Fig. 10, where eight repetitions have been considered. The numbers obtained for τ are coherent with what has been observed when performing the experiments, delivering estimates ranging from 1.44 to 3.58 seconds. Values inside this range depend both on the actual speed of the masses and on where they actually hit the fiber. Considering an average distance of two to three meters between the point where the masses touch the first fiber and the second, the mean speed values would be around 0.8 and 1.3 m/s, similar to a walking person's velocity, which is reasonable. By adding more monitored fibers in the same space, or just better displacing two so that the space uncertainty is reduced, the τ estimate accuracy would be enhanced. False alarm probability, by means of a proper algorithm, would be further reduced in this scenario

V. Discussion and Conclusions

This work presents an experimental on-field demonstration of a realistic polarization-based optical fiber sensing system, for the early warning of potentially dangerous mass transport phenomena in mountain scenarios. The system has been characterized under different configurations and operating conditions. First, we ensured that the section of installed fiber used to connect the interrogator to the monitoring site would not introduce, in normal conditions, false alarms due to ordinary events such as vehicular traffic or people and animals passing by. We characterized the SOP angular speed evolution in time showing that a low SOPAS level can be maintained also for long observation times and for all the tested fiber layout configurations, including a sensing fiber up to 80 m long. The system proved to be sensitive to common circumstances such as walking over a semi-exposed section of the fiber cable, but we also showed that resulting SOPAS levels are well below what can be reasonably expected to be the effect of intense debris flows on the SOP variation.

Moreover, we have emulated rockfall events by dropping a set of spherical masses from the top of the gully and let them roll over a sensing fiber 40 m long. Our findings show that the generated SOPAS peaks are about two orders of magnitude higher than the average noise level measured for both 40 m and 80 m long fibers, thus confirming that a threshold-based algorithm can efficiently distinguish regular operating conditions from hazardous events that would result in much higher SOP variations and longer duration time than those that we were able to induce in our experiments.

Lastly, we implemented a two-fiber solution to demonstrate the potential for improved system performance in terms of robustness to false alarms. We again emulated rockfalls on the gully where two fibers where deployed in two different areas. By using one polarimeter for each of the fiber we were able to detect the same rockfall occurrence on the two fibers separately. This would allow triggering an alarm only when the event is detected also on the second (bottom) fiber, thus further reducing the probability of false alarms. Furthermore, this study opens the way for an even more efficient solution where more than two fibers are monitored by the same polarimeter thanks to a low-cost (hundreds of €) optical switch at the polarimeter input, as we have shown in [21]. This configuration enables a rough estimation of the event location when the fibers are installed in different portions of the same site, or a considerable cost reduction when different fibers are used to monitor different sites with the same hardware components.

The results shown in this paper, in our opinion, lay further more consistent groundwork for a working monitoring system completely relying on polarization. The configuration tested in this manuscript was somehow worst-case for the characterization of the background noise and could be subject to serious damages in the case of a rockfall event. We envision that a future development of this sensing system should probably employ buried fiber cables over the gully, so that environmental noise can be further reduced, without really affecting the sensitivity to real events, which would be much more intense than small masses rolling over the site, which we used in our experiments. Another option can be to install the fiber longitudinally along the mountain slope, laterally displaced with respect to the center of the gully [21], to prevent damages due to massive debris flowing along the center of the gully. Moreover, the whole fiber can be divided in different shorter spans joined together through fiber

connectors and alternated with fiber sections crossing the gully transversally to improve detection. Using this configuration, a flowing mass might only affect portions of the fiber and not the whole installation. One or a few fiber spans would need to be replaced thus reducing re-installation efforts and costs.

REFERENCES

[1] M. Arattano and L. Marchi, "Systems and sensors for debris-flow monitoring and warning," *Sensors*, vol. 8, no. 4, pp. 2436–2452, 2008.

[2] M. Hürlimann et al., "Debris-flow monitoring and warning: Review and examples," *Earth- Sci. Rev.*, vol. 199, 2019, Art. no. 102981.

[3] S.-C. Wei and K.-F. Liu, "Automatic debris flow detection using geophones," *Landslides*, vol. 17, no. 2, pp. 349–359, 2020.

[4] K. Takahashi, D. Mecatti, D. Dei, M. Matsumoto, and M. Sato, "Landslide observation by ground-based SAR interferometry," in *Proc. IEEE Int. Geosci. Remote Sens. Symp.*, 2012, pp. 6887–6890.

[5] A. Martinez-Vazquez and J. Fortuny-Guasch, "A GB-SAR processor for snow avalanche identification," *IEEE Trans. Geosci. Remote Sens.*, vol. 46, no. 11, pp. 3948–3956, Nov. 2008.

[6] J. Aaron, R. Spielmann, B. W. McArdell, and C. Graf, "High-frequency 3D LiDAR measurements of a debris flow: A novel method to investigate the dynamics of full-scale events in the field," *Geophysical Res. Lett.*, vol. 50, no. 5, 2023, Art. no. e2022GL102373.

[7] M. V. Ramesh and N. Vasudevan, "The deployment of deep-earth sensor probes for landslide detection," *Landslides*, vol. 9, no. 4, pp. 457–474, 2012.

[8] A. H. Hartog, *An Introduction to Distributed Optical Fibre Sensors*. Boca Raton, FL, USA: CRC Press, 2017.

[9] B. Culshaw and A. Kersey, "Fiber-optic sensing: A historical perspective," *J. Lightw. Technol.*, vol. 26, no. 9, pp. 1064–1078, May 2008.

[10] Z.-Y. Dai, Y. Liu, L.-X. Zhang, Z.-H. Ou, C. Zhou, and Y.-Z. Liu, "Landslide monitoring based on high-resolution distributed fiber optic stress sensor," in *Proc. IEEE 1st Asia-Pacific Opt. Fiber Sensors Conf.*, 2008, pp. 1–4.

[11] L. Schenato, "A review of distributed fibre optic sensors for geo-hydrological applications," *Appl. Sci.*, vol. 7, no. 9, 2017, Art. no. 896.

[12] L. Schenato, A. Pasuto, A. Galtarossa, and L. Palmieri, "On the use of OFDR for high-spatial resolution strain measurements in mechanical and geotechnical engineering," in *Proc. IEEE Int. Instrum. Meas. Technol. Conf.*, 2018, pp. 1–6.

[13] Y. Muanenda, C. J. Oton, S. Faralli, and F. Di Pasquale, "A cost-effective distributed acoustic sensor using a commercial off-the-shelf DFB laser and direct detection phase-OTDR," *IEEE Photon. J.*, vol. 8, no. 1, Feb. 2016, Art. no. 6800210.

[14] Y. Koyamada, M. Imahama, K. Kubota, and K. Hogari, "Fiber-optic distributed strain and temperature sensing with very high measurand resolution over long range using coherent OTDR," *J. Lightw. Technol.*, vol. 27, no. 9, pp. 1142–1146, May 2009.

[15] J. Pastor-Graells, H. F. Martins, A. Garcia-Ruiz, S. Martin-Lopez, and M. Gonzalez-Herraez, "Single-shot distributed temperature and strain tracking using direct detection phase-sensitive OTDR with chirped pulses," *Opt. Exp.*, vol. 24, no. 12, pp. 13121–13133, Jun. 2016. [Online]. Available: https://opg.optica.org/oe/abstract.cfm?URI=oe-24-12-13121

[16] I. Di Luch, P. Boffi, M. Ferrario, G. Rizzelli, R. Gaudino, and M. Martinelli, "Vibration sensing for deployed metropolitan fiber infrastructure," *J. Lightw. Technol.*, vol. 39, no. 4, pp. 1204–1211, Feb. 2021.

[17] I. Di Luch, M. Ferrario, G. Rizzelli, R. Gaudino, and P. Boffi, "Vibration sensing for deployed metropolitan fiber infrastructures," in *Proc. Opt. Fiber Commun. Conf. Exhib.*, 2020, pp. 1–3.

[18] I. Di Luch, M. Ferrario, P. Boffi, G. Rizzelli, H. Wang, and R. Gaudino, "Demonstration of structural vibration sensing in a deployed PON infrastructure," in *Proc. IEEE 45th Eur. Conf. Opt. Commun.*, 2019, pp. 1–3.

[19] S. Pellegrini, G. Rizzelli, M. Barla, and R. Gaudino, "Algorithm optimization for rockfalls alarm system based on fiber polarization sensing," *IEEE Photon. J.*, vol. 15, no. 3, Jun. 2023, Art. no. 7100709.

[20] S. Aiassa et al., "A new real-time debris flow and avalanches detection system based on optical fiber sensing," in *Proc. 8th Int. Conf. Debris Flow Hazard Mitigation*, 2023, Art. no. 03001.

[21] G. Rizzelli et al., "Early-warning debris flow and avalanches detection system based on optical fiber polarization sensing," in *Proc. IEEE 23rd Int. Conf. Transparent Opt. Netw.*, 2023, pp. 1–4.

[22] K. Okamoto, T. Edahiro, and N. Shibata, "Polarization properties of single-polarization fibers," *Opt. Lett.*, vol. 7, no. 11, pp. 569–571, Nov. 1982. [Online]. Available: https://opg.optica.org/ol/abstract.cfm?URI=ol-7-11-569

[23] K. Okamoto, *Fundamentals of Optical Waveguides*. Amsterdam, The Netherlands: Elsevier, 2006.

[24] L. Palmieri and A. Galtarossa, "Coupling effects among degenerate modes in multimode optical fibers," *IEEE Photon. J.*, vol. 6, no. 6, Dec. 2014, Art. no. 0600408.

[25] E. Frins and W. Dultz, "Rotation of the polarization plane in optical fibers," *J. Lightw. Technol.*, vol. 15, no. 1, pp. 144–147, Jan. 1997.

[26] R. Ulrich, S. C. Rashleigh, and W. Eickhoff, "Bending-induced birefringence in single-mode fibers," *Opt. Lett.*, vol. 5, no. 6, pp. 273–275, Jun. 1980. [Online]. Available: https://opg.optica.org/ol/abstract.cfm?URI=ol-5-6-273

[27] J. Sakai and T. Kimura, "Birefringence and polarization characteristics of single-mode optical fibers under elastic deformations," *IEEE J. Quantum Electron.*, vol. JQE-17, no. 6, pp. 1041–1051, Jun. 1981.

[28] R. Ulrich and A. Simon, "Polarization optics of twisted single-mode fibers," *Appl. Opt.*, vol. 18, no. 13, pp. 2241–2251, Jul. 1979. [Online]. Available: https://opg.optica.org/ao/abstract.cfm?URI=ao-18-13-2241

[29] A. Mecozzi, M. Cantono, J. C. Castellanos, V. Kamalov, R. Muller, and Z. Zhan, "Polarization sensing using submarine optical cables," *Optica*, vol. 8, no. 6, pp. 788–795, Jun. 2021.

[30] A. Mecozzi et al., "Use of optical coherent detection for environmental sensing," *J. Lightw. Technol.*, vol. 41, no. 11, pp. 3350–3357, Jun. 2023.

[31] S. Pellegrini, R. Gaudino, and C. Crognale, "Experimental demonstration of vibration sensing and positioning on multiple metropolitan fibers," in *Proc. IEEE Photon. Soc. Summer Topicals Meeting Ser.*, 2023, pp. 1–2.

[32] M. Farin, V. C. Tsai, M. P. Lamb, and K. E. Allstadt, "A physical model of the high-frequency seismic signal generated by debris flows," *Earth Surf. Processes Landforms*, vol. 44, no. 13, pp. 2529–2543, 2019.

[33] J. Liu, S. Yuan, Y. Dong, B. Biondi, and H. Y. Noh, "TelecomTM: A fine-grained and ubiquitous traffic monitoring system using pre-existing telecommunication fiber-optic cables as sensors," *Proc. ACM Interact. Mobile Wearable Ubiquitous Technol.*, vol. 7, no. 2, pp. 1–24, Jun. 2023. [Online]. Available: https://doi.org/10.1145/3596262

[34] N. J. Lindsey, S. Yuan, A. Lellouch, L. Gualtieri, T. Lecocq, and B. Biondi, "City-scale dark fiber DAS measurements of infrastructure use during the COVID-19 pandemic," *Geophysical Res. Lett.*, vol. 47, no. 16, 2020, Art. no. e2020GL089931. [Online]. Available: https://agupubs.onlinelibrary.wiley.com/doi/abs/10.1029/2020GL089931

[35] V. Coviello, M. Arattano, F. Comiti, P. Macconi, and L. Marchi, "Seismic characterization of debris flows: Insights into energy radiation and implications for warning," *J. Geophysical Res., Earth Surf.*, vol. 124, no. 6, pp. 1440–1463, 2019. [Online]. Available: https://agupubs.onlinelibrary.wiley.com/doi/abs/10.1029/2018JF004683

Open Access funding provided by 'Politecnico di Torino' within the CRUI CARE Agreement